

On the Adsorption Mechanism of Caffeine on MAPbI₃ Perovskite Surfaces: A Combined UMC–DFT Study

Luiz A. Ribeiro Júnior^{a,b,*}, Raphael M. Tromer^c, Ramiro M. dos Santos^a and Douglas S. Galvão^{c,d}

^a*Institute of Physics, University of Brasília, 70910-900, Brasília, Brazil*

^b*PPGCIMA, Campus Planaltina, University of Brasília, 73345-010, Brasília, Brazil*

^c*Applied Physics Department, University of Campinas, Campinas, São Paulo, Brazil.*

^d*Center for Computing in Engineering and Sciences, University of Campinas, Campinas, São Paulo, Brazil.*

ARTICLE INFO

Keywords:

UMC–DFT Simulations
MAPbI₃ Perovskite
Caffeine
Molecular Dye
Adsorption
Solar Cells

ABSTRACT

Recently, it was experimentally shown that the performance and thermal stability of the perovskite MAPbI₃ were improved upon the adsorption of a molecular layer of caffeine. In this work, we used a hybrid methodology that combines Uncoupled Monte Carlo (UMC) and Density Functional Theory (DFT) simulations to carry out a detailed and comprehensive study of the adsorption mechanism of a caffeine molecule on the surface of MAPbI₃. Our results showed that the adsorption distance and energy of a caffeine molecule on the MAPbI₃ surface are 2.0 Å and -0.3 eV, respectively. The caffeine/MAPbI₃ complex presents a direct bandgap of 2.38 eV with two flat intragap bands distanced 1.15 and 2.18 eV from the top of valence bands. Although the energy band levels are not significantly shifted by the presence of caffeine, the interaction MAPbI₃/perovskite is enough to affect the bands' dispersion, particularly the conduction bands.

1. Introduction

The achievements obtained in producing a more efficient third-generation of solar cells were fundamental for the recent advances in photovoltaics [1–5]. Nowadays, this new generation of photovoltaic technology, with low cost and potential fast production on a large scale, has as one of the protagonists the organic-inorganic halide perovskites [6–11]. Among these perovskites, the most studied material is MAPbI₃ (where MA refers to methylamine) [12–23]. The success of this material in manufacturing solar cells is attributed to some of its outstanding properties such as suitable bandgap for optoelectronics applications, high photon absorption coefficient, fast exciton to polaron conversion (due to very low binding energy for excitons), and the long lifetime presented by free charge carriers [6, 10]. Although MAPbI₃ possesses interesting properties for photovoltaic applications, the problem of low photo and thermal stability are still drawbacks for its large-scale use [10, 12, 21].

Recently, experimental investigations proposed improvements in the thermal stability of perovskite-based solar cells (PSCs) upon the doping or adsorption of small molecules (molecular dyes) on their surfaces [4, 23–31]. One of the aims of these studies was to address the fast degradation of these perovskite species when exposed to environmental factors. Wang and colleagues showed that the adsorption of caffeine molecules improved the performance and thermal stability of PSCs based on MAPbI₃ layers [23, 32]. Their findings revealed that the strong interaction between caffeine

✉ ribeirojr@unb.br (L.A.R. Júnior)

ORCID(s):

and Pb²⁺ ions serves as a “molecular lock” that increases the activation energy during film crystallization, yielding a perovskite film with a preferred orientation, improved electronic properties, greatly enhanced thermal stability, and a stabilized power conversion efficiency (PCE) of 19.8% [23]. Albeit some dye-sensitized PSCs have been proposed recently with improved PCE [26, 29, 30], the adsorption mechanisms between molecular dyes on perovskite layers remain not fully understood.

In the present work — inspired by the recent progress in obtaining MAPbI₃-based PSCs with improved performance upon caffeine doping [23, 32] — we carried out uncoupled Monte Carlo (UMC) and density functional theory (DFT) simulations to study the structural and electronic properties of the caffeine/MAPbI₃ complex. Caffeine and MA (methylammonium) have the following chemical formulas C₈H₁₀N₄O₂ and CH₃NH₃, respectively. This hybrid methodology showed a good compromise between computational cost and accuracy [33]. From the UMC realizations, the caffeine/MAPbI₃ conformation of the lowest interaction energy is obtained. DFT calculations were used to obtain the electronic properties of this structure. In this way, by combining UMC and DFT methodologies we proposed a more detailed and comprehensive description of the adsorption mechanism of caffeine molecules on MAPbI₃ layers [32], contributing to further understand the interaction between these species.

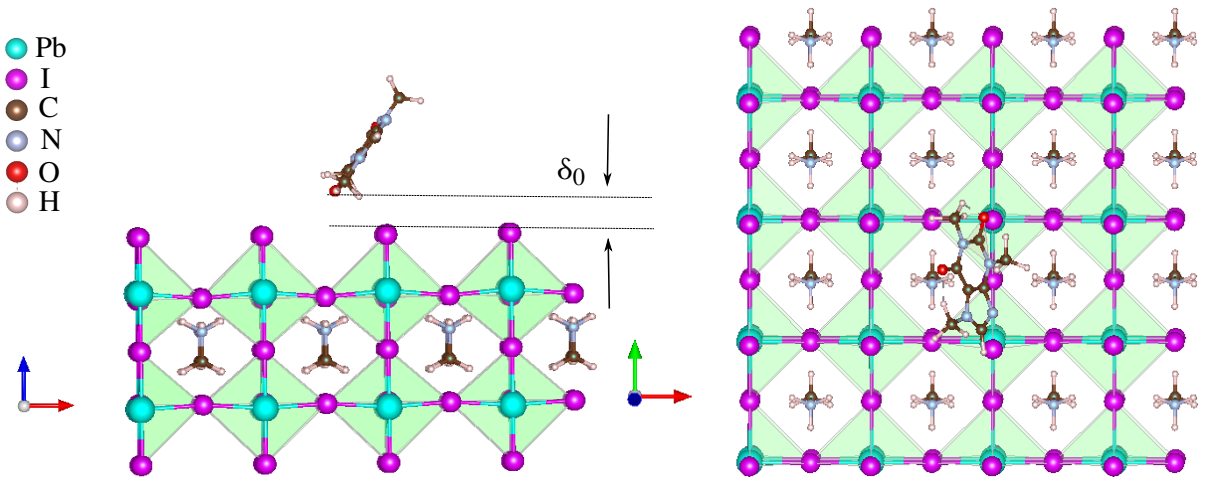


Figure 1: Schematic representation of the DFT optimized caffeine/MAPbI₃ structure. The left panel illustrates the side view whereas the right panel shows the top view. The color scheme for the atoms is presented within the figure. Caffeine and MA (methylammonium) have the following chemical formulas C₈H₁₀N₄O₂ and CH₃NH₃, respectively. δ_0 is the distance between this molecule to the perovskite surface after the geometry optimization (2.0 Å).

2. Methodology

For the description of the structural and electronic properties of a caffeine molecule adsorbed on a MAPbI₃ layer, we used UMC (Adsorption Locator Modulus) as implemented in Materials Studio [34–37]. The DFT calculations were carried out using the SIESTA code [38]. The UMC approach samples several configurations in the canonical ensemble

by generating a large set of caffeine/MAPbI₃ systems, starting from a trial (random) configuration. The arrangement of these conformations is randomly chosen by rotating and translating the molecule (caffeine) about an axis fixed by a substrate (MAPbI₃ layer). The search for the lowest energy configurations is obtained by using the simulated annealing method. The Metropolis algorithm provides the statistical weights employed in this scheme [37]. Here, the parameters used in the annealing procedure were: 50000 annealing cycles, 300 K for the initial temperature, 500 K for the mid-cycle temperature, 5 heating ramps per cycle, 100 dynamic steps per ramp, and 5000 for the total number of steps. These parameters were used before to simulate the interaction between a pentacene dimer [33]. Importantly, a satisfactory number of conformations (100) were considered. The UMC mentioned above was repeated 100 times to obtain the best set of minimum-energy configurations. This UMC protocol yields the system conformation with the lowest interaction energy (see Figure 1). There are two other possible configurations, with MA or Pb ions covering (see Figures S1 and S2(a) in the Supplementary Material). The configuration in 1 is the most stable one [23, 32]. We take these complexes to study the electronic properties of the caffeine molecule adsorbed on MAPbI₃.

When it comes to the DFT calculations, a good simulation performance in describing a system containing the Pb²⁺ ion is achieved using single zeta polarized basis functions [39]. Relativistic pseudopotentials were also used [40], with core correction and parameterized by Troullier-Martins' method [41]. The exchange-correlation energies were approximated by the GGA functional, using Becke's exchange functional methodology [42], and Lee-Yang-Parr correlation (BLYP) [43]. The BLYP functional was successfully used to calculate the electronic structure properties of perovskites [44, 45]. The cut-off energy was settled as 500 Ry. Due to the large value of the lattice parameters, we have employed a $15 \times 15 \times 5$ Monkhorst-Pack mesh to better describe the properties within a volume in the reciprocal lattice [46]. Importantly, the lowest energy configuration yielded in UMC simulations was optimized using DFT and the final MA orientation was practically unaltered, while, as expected, the perovskite geometry is slightly different.

3. Results

We begin our discussions by examining the crystal structure for the caffeine/MAPbI₃ configuration after the dye adsorption. Figure 1 shows the DFT optimized geometry for the caffeine/MAPbI₃ complex. δ_0 is the distance between this molecule to the perovskite surface (Iodine atoms) after the geometry optimization 2.0 Å. The perovskite present cubic structure with supercell dimensions of $25.57 \text{ Å} \times 25.57 \text{ Å} \times 56.7 \text{ Å}$ for the x, y, and z directions, respectively. The value along the z-direction is large enough to prevent spurious interactions between the image layers. The Pb-I distances are 3.20 Å and 3.22 Å along the x and y directions, respectively, and 2.90 Å for z-direction. The forces converged until reaching a minimum value of $1.0 \times 10^{-3} \text{ eV/Å}$. To ensure a good compromise between the accuracy of our results and the computational feasibility, the tolerance in the matrix and the total energy was set at 1.0×10^{-4} and $1.0 \times 10^{-5} \text{ eV}$, respectively.

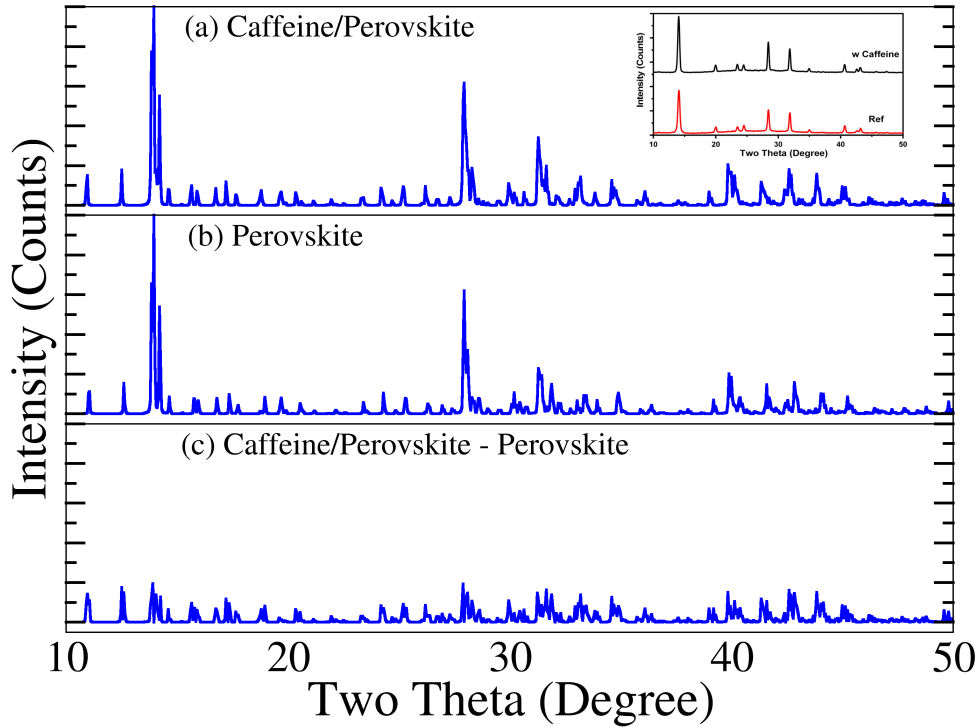


Figure 2: Simulated X-ray diffraction pattern for the caffeine/MAPbI₃ configuration at 300 K, after the dye adsorption. (a) The complex perovskite/caffeine, (b) isolated perovskite, (c) the difference between the data shown in (a) and (b)

. The inset panel shows the XRD measurements obtained in reference [23].

Figure 2(a) depicts the simulated X-ray diffraction (XRD) pattern for this configuration at 300 K. Figures 2(b) and 2(c) show the XRD pattern for the isolated perovskite layer and for the difference between the cases 2(b) and 2(c), respectively. The XRD pattern was obtained by using the Reflex module as implemented in Materials Studio [47–49]. These XRD patterns were simulated using the optimized structure presented in Figure 2. It was used as a benchmark that our results are consistent with the experimental one. In our calculations, we used a single crystal and the following diffractometer parameters: a two theta range of [5–45] degrees with a step size of 0.05 degrees; the distance between the planes of atoms that give rise to diffraction peaks ($1/d$) were settled to 0.056628 and 0.49681 for the minimum and maximum theta two values, respectively; and the Bragg–Brentano geometry was employed. For the radiation, we used in the simulations a copper source, $\lambda_1 = 1.540 \text{ \AA}$, $\lambda_2 = 1.544 \text{ \AA}$, $I_2/I_1 = 0.50$ (the intensity ratio of the x-rays corresponding to the wavelengths λ_2 and λ_1 , respectively), and polarization of 0.5 (that specifies the fraction of the x-ray beam polarized in the direction perpendicular to the plane of the incident and diffracted beams).

The inset panel shows the XRD measurements obtained in reference [23]. We can see that the simulated XRD pattern shows a good agreement with the experimental one [23], even considering the adsorption mechanism of a single caffeine molecule on top of a MAPbI₃ surface. The calculated reflection peaks occur at approximately 14.02° ,

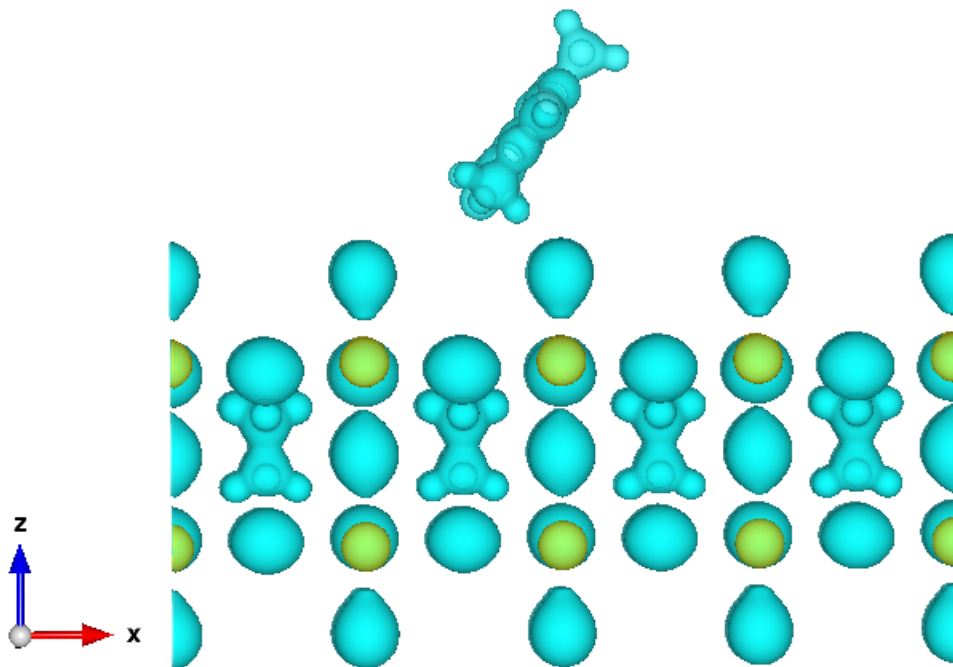


Figure 3: Schematic representation of the electrostatic potential of caffeine/perovskite. Green and cyan represent negative and positive values, respectively.

very close to the ones reported in the experiments (13.90°, inset panel in Figure 2) [28]. This XRD pattern points to a tetragonal perovskite phase with the dominant (110) lattice reflection at 14.02°, which is the preferred orientation for the perovskite films [23]. These results show that our combined UMC–DFT approach can accurately describe the adsorption configuration of molecular dyes on the surface of MAPbI₃ layers. As expected, the caffeine adsorption does not significantly affect the main peaks associated with MAPbI₃ since caffeine remains on the surface (no intercalation), as shown in Figure 2(c).

To quantify the interaction between caffeine and MAPbI₃, we have calculated the DFT adsorption energies according to the expression $E_a = [E_{pc} - (E_p + E_c)]$, where E_{pc} , E_p , and E_c are the total energies for the caffeine/MAPbI₃ configuration after the dye adsorption, isolated MAPbI₃ monolayer, and isolated caffeine molecule, respectively. The DFT estimated adsorption energy is $E_a = -0.3$ eV.

Figure 3 illustrates the electrostatic potential over the structure. Due to this electrostatic potential configuration, the caffeine molecule is adsorbed on the perovskite structure by interacting with I[−] and the Pb²⁺ ions, which contributes to the stability of the structure. As claimed by Wang *et al.* [23, 32], it is this strong Pb²⁺/caffeine interaction that works as a “molecular lock” enhancing the structural stability. It is important to stress that although the E_a is larger for the case of MA covering (−1.14 eV), in this configuration the MA molecules can easily evaporate, which compromises the overall structural gain. For the Pb covering case, this configuration is structurally unstable (see Figure S2 (b) in the

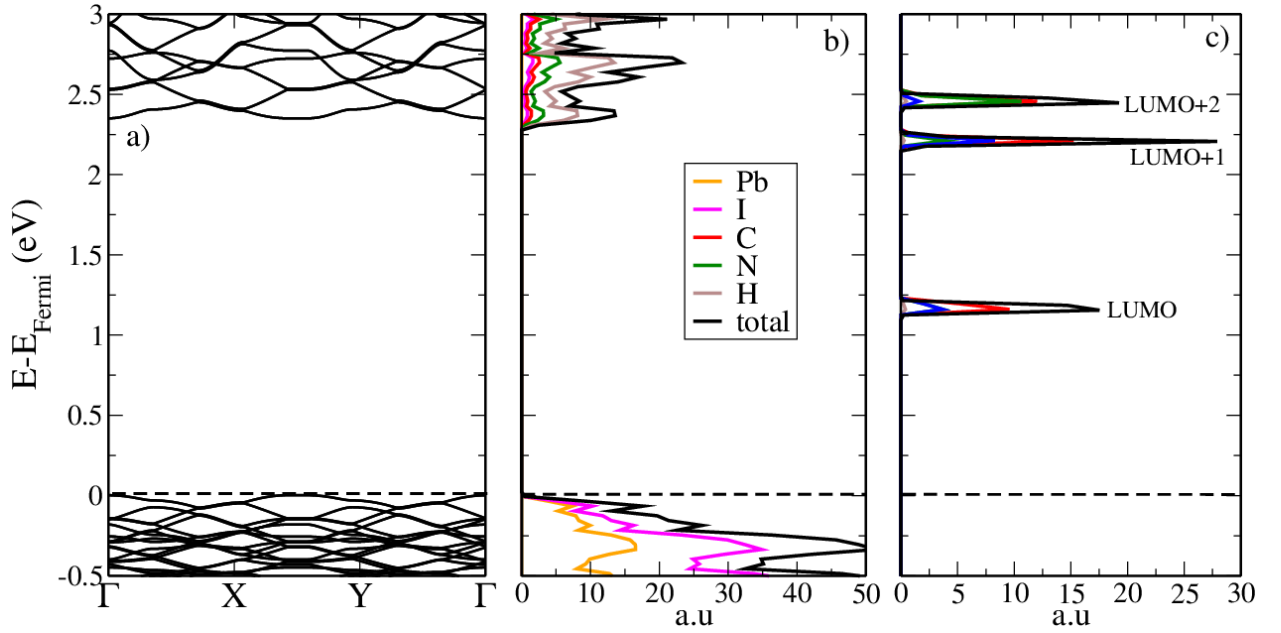


Figure 4: (a) Electronic band structure and (b) the corresponding projected density of states (PDOS) for the isolated MAPbI₃ perovskite. (c) LUMO, LUMO+1, and LUMO+2 molecular orbitals for the isolated caffeine.

Supplemental Material).

Now we present the electronic band structure (Figure 4 (a)) and the corresponding projected density of states (PDOS) (Figure 4 (b)) for the isolated MAPbI₃ slab. In Figure 4 (c), we show the LUMO, LUMO+1, and LUMO+2 states for the isolated caffeine molecule. LUMO refers to Lowest Unoccupied Molecular Orbital. In Figure 4(a), we can observe a direct bandgap of about 2.4 eV at the gamma point. This value agrees with the ones reported in the literature for other theoretical studies [50, 51]. It should be stressed that, in general, GGA tends to underestimate the bandgap values. However, there are a few cases in which GGA predicted band gaps in good agreement with experiments. For example, it was reported a calculated bandgap of about 1.6 eV for MAPbI₃ employing PBE-GGA [52] (probably due to error cancellations). There are also GGA studies where the perovskite bandgap values are overestimated [52], as in our case. Here, we have also tested other MAPbI₃ slabs (see Supplemental Material). The obtained bandgap value for the stable configuration (MA covering) is about 1.4 eV. We can see from the PDOS of the slab that I and Pb atoms have a large contribution to the valence bands, while the I and H atoms to the conduction ones. For the sake of comparison, we show in Figure 4 (c) the LUMO, LUMO+1, and LUMO+2 molecular orbitals for the isolated caffeine.

In Figure 5 we present the electronic band structure 5(a) and the corresponding PDOS 5(b) of the caffeine/MAPbI₃ complex. Besides, we included in Figure 5(c) the contributions of the caffeine atoms to the PDOS complex. Upon the caffeine adsorption, the MAPbI₃ bandgap is almost the same, with the appearance of two midgap flat bands (LUCO and LUCO+1, distanced 1.15 and 2.18 eV from the HOCO bands. HOCO and LUCO refer to the Highest/Lowest

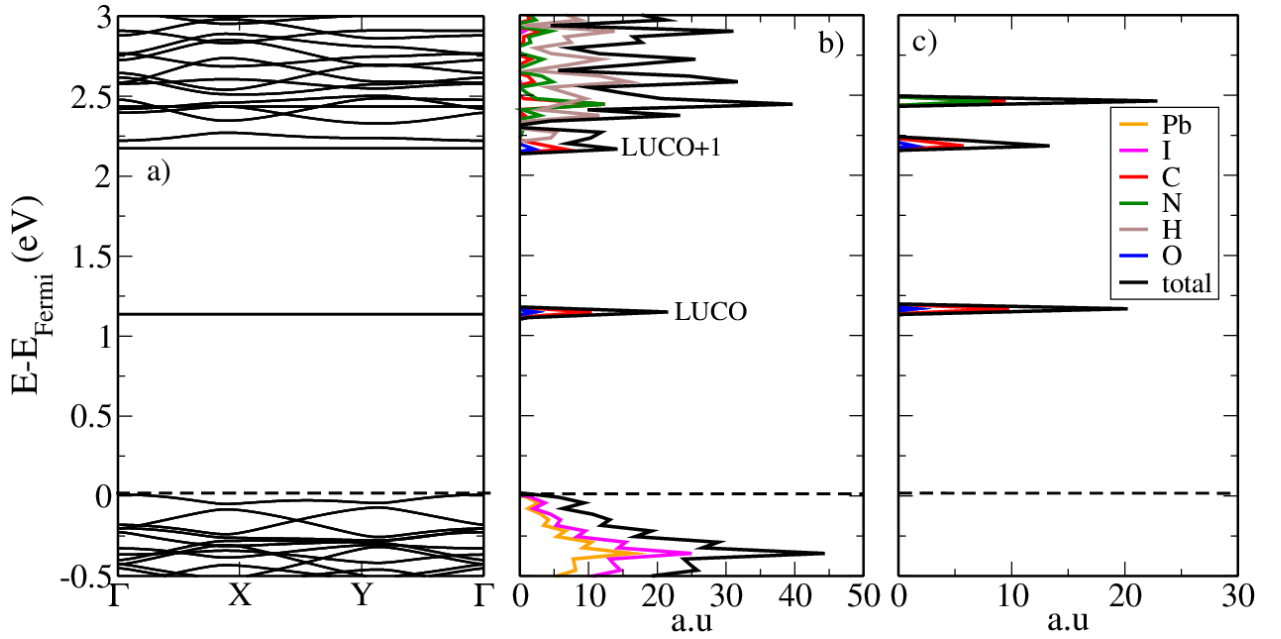


Figure 5: (a) Electronic band structure and (b) the corresponding projected density of states (PDOS) for the MAPbI₃/caffeine system. (c) The contribution of the caffeine atoms to the PDOS.

Occupied/Unoccupied Crystalline Orbitals, respectively. These flat bands can be attributed to caffeine and have almost the same energy values from the molecular case (Figure 4(c)). Since the momentum conservation of the excited electron upon photon absorption is characterized by the presence of a direct bandgap, the vertical (direct) transitions of this excited electron can form excitons spontaneously. The presence of flat midgap states favors the formation of excitons with considerably lower binding energy. These excitons are easily dissociated in the material due to the weak interaction between the electron-hole pair. We see from PDOS of caffeine/MAPbI₃ complex (Figure 5(b)) that Pb and I atoms have large contributions to the valence bands, while the non-metal atoms have larger contributions to the conduction bands. As discussed below, there is a charge transfer of $-0.1e$ from caffeine to perovskite. Although this charge amount is not enough to significantly change the energy band positions, it is enough to affect the band's dispersion, as evidenced by contrasting Figures 4(a) and 5(a).

Finally, Figure 6 shows (a) LUMO and (b) LUMO+1 (frontier orbitals) for an isolated caffeine molecule and, (c) LUCO+1 of the caffeine/MAPbI₃ complex. Figure 6(d) depicts the isosurface charge density. The LUMO (isolated caffeine) and LUCO (complex, not shown in this figure) present similar orbital configurations (the LUMO is illustrated in Figure 6(a)). On the other hand, the LUMO+1 (isolated caffeine) and LUCO+1 (complex) differ substantially when it comes to their distribution. Upon adsorption, as mentioned above, it occurs a charge transfer from caffeine to the perovskite. This charge transference is responsible for changing the orbital configurations of the related LUMO+1 and LUCO+1 levels. Figure 6(d) shows a top view of the system presented in Figure 1 with its related isosurfaces. This

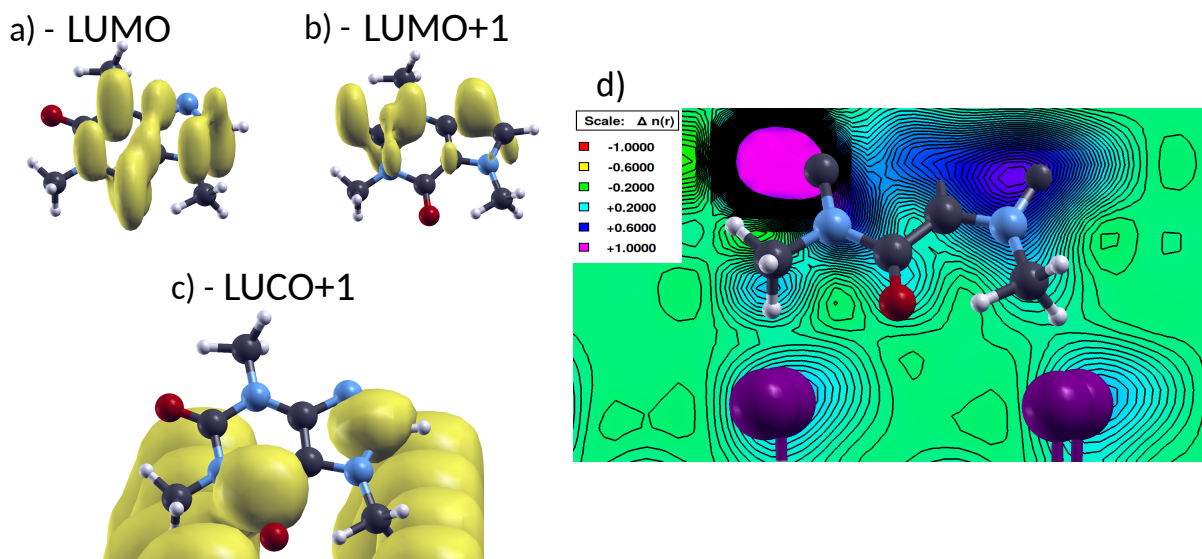


Figure 6: (a) LUMO and (b) LUMO+1 (frontier orbitals) for an isolated caffeine molecule and, (c) LUCO+1 of the caffeine/MAPbI₃ complex. (d) depicts the isosurfaces charge density. The color code represents the values of the electronic densities ($\Delta n(r)$). The pink and red colors refer to the maximum ($+1e$, hole) and minimum ($-1e$, electron) electronic densities, respectively.

particular view hides almost all the perovskite surface — just 4 Iodine atoms (purple spheres) can be visualized — and also some atoms of the caffeine molecule. The colors in Figure 6(d) denote the local variation in the electronic density ($\Delta n(r)$). In the adopted color code, the pink and red colors refer to the maximum ($+1e$, hole) and minimum ($-1e$, electron) electronic densities, respectively. The other colors stand for intermediate values for the electronic densities. One can note a continuous isosurface enveloping the hydrogen atoms (white spheres) and the Iodine ones (purple spheres), which shows the interaction channels between caffeine and perovskite for the model complex studied here.

4. Conclusions

In summary, we used a hybrid methodology that combined uncoupled Monte Carlo and density functional theory simulations to study the structural and electronic properties of a caffeine molecule adsorbed on the surface of MAPbI₃ perovskite. Our findings showed that the adsorption distance and adsorption energy of a caffeine molecule on the MAPbI₃ surface are 2.0 Å and -0.3 eV, respectively. The calculated X-ray diffraction pattern at 300 K showed a good agreement with the experimental one. The calculated reflection peak occurs at approximately 14.02°, very close to the one reported in experiments (13.90°) [28]. Moreover, the electrostatic potential analysis revealed that the caffeine molecule is adsorbed on the perovskite structure due to its strong interaction with the Pb²⁺ ions, with a charge transfer of 0.1e from caffeine to perovskite. The caffeine/MAPbI₃ complex presents a direct bandgap of 2.38 eV with two flat intragap bands distanced 1.15 and 2.18 eV from the top of valence bands. Although the energy band levels are

not significantly shifted by the presence of caffeine, the interaction MAPbI₃/perovskite is enough to affect the band's dispersion, particularly the conduction bands. Although the E_a is larger for the case of MA covering (-1.14 eV), in this configuration the MA molecules can easily evaporate, which compromises the overall structural gain. For the Pb covering case, this configuration is structurally unstable. Pb and I atoms have large contributions to the valence bands, while the non-metal atoms have larger contributions to the conduction bands. We found a charge transfer of $-0.1e$ from caffeine to perovskite. Although this charge amount was not enough to significantly change the energy band positions, it was enough to affect the band structure dispersion. The improvements on the perovskite quality samples due to the caffeine presence were already unambiguously experimentally established [23, 32]. Our results from *ab initio* calculations and Monte Carlo techniques provide deeper insights into the structural and electronic aspects of the caffeine presence. We hope the present work can stimulate further studies on other dyes.

Acknowledgments

The authors gratefully acknowledge the financial support from Brazilian Research Councils CNPq, CAPES, and FAPDF and CENAPAD-SP for providing the computational facilities. L.A.R.J. gratefully acknowledges respectively, the financial support from FAP-DF and CNPq grants 00193.0000248/2019 – 32 and 302236/2018 – 0. D.S.G. thank the Center for Computing in Engineering and Sciences at Unicamp for financial support through the FAPESP/CEPID Grants #2013/08293–7 and #2018/11352–7. L.A.R.J. gratefully acknowledges the financial support from DPI/DIRPE (Edital 03/2020) grant 23106.057541/2020–89 and from IFD/UnB (Edital 01/2020) grant 23106.090790/2020–86.

References

- [1] Martin A Green. Third generation photovoltaics: solar cells for 2020 and beyond. *Physica E: Low-dimensional Systems and Nanostructures*, 14(1-2):65–70, 2002.
- [2] Arthur J Nozik, Matthew C Beard, Joseph M Luther, Matt Law, Randy J Ellingson, and Justin C Johnson. Semiconductor quantum dots and quantum dot arrays and applications of multiple exciton generation to third-generation photovoltaic solar cells. *Chemical reviews*, 110(11):6873–6890, 2010.
- [3] Gavin Conibeer, Martin Green, Richard Corkish, Young Cho, Eun-Chel Cho, Chu-Wei Jiang, Thipwan Fangsuwannarak, Edwin Pink, Yidan Huang, Tom Puzzer, et al. Silicon nanostructures for third generation photovoltaic solar cells. *Thin solid films*, 511:654–662, 2006.
- [4] Norasikin A Ludin, AM Al-Alwani Mahmoud, Abu Bakar Mohamad, Abd Amir H Kadhum, Kamaruzzaman Sopian, and Nor Shazlinah Abdul Karim. Review on the development of natural dye photosensitizer for dye-sensitized solar cells. *Renewable and Sustainable Energy Reviews*, 31:386–396, 2014.
- [5] Albert Polman and Harry A Atwater. Photonic design principles for ultrahigh-efficiency photovoltaics. *Nature materials*, 11(3):174–177, 2012.
- [6] Martin A Green, Anita Ho-Baillie, and Henry J Snaith. The emergence of perovskite solar cells. *Nature photonics*, 8(7):506–514, 2014.

- [7] Mingzhen Liu, Michael B Johnston, and Henry J Snaith. Efficient planar heterojunction perovskite solar cells by vapour deposition. *Nature*, 501(7467):395–398, 2013.
- [8] Huanping Zhou, Qi Chen, Gang Li, Song Luo, Tze-bing Song, Hsin-Sheng Duan, Ziruo Hong, Jingbi You, Yongsheng Liu, and Yang Yang. Interface engineering of highly efficient perovskite solar cells. *Science*, 345(6196):542–546, 2014.
- [9] Henry J Snaith, Antonio Abate, James M Ball, Giles E Eperon, Tomas Leijtens, Nakita K Noel, Samuel D Stranks, Jacob Tse-Wei Wang, Konrad Wojciechowski, and Wei Zhang. Anomalous hysteresis in perovskite solar cells. *The journal of physical chemistry letters*, 5(9):1511–1515, 2014.
- [10] Juan-Pablo Correa-Baena, Michael Saliba, Tonio Buonassisi, Michael Grätzel, Antonio Abate, Wolfgang Tress, and Anders Hagfeldt. Promises and challenges of perovskite solar cells. *Science*, 358(6364):739–744, 2017.
- [11] Hsinhan Tsai, Wanyi Nie, Jean-Christophe Blancon, Constantinos C Stoumpos, Reza Asadpour, Boris Harutyunyan, Amanda J Neukirch, Rafael Verduzco, Jared J Crochet, Sergei Tretiak, et al. High-efficiency two-dimensional Ruddlesden–Popper perovskite solar cells. *Nature*, 536(7616):312–316, 2016.
- [12] Yongzhen Wu, Fengxian Xie, Han Chen, Xudong Yang, Huimin Su, Molang Cai, Zhongmin Zhou, Takeshi Noda, and Liyuan Han. Thermally stable mapbi3 perovskite solar cells with efficiency of 19.19% and area over 1 cm² achieved by additive engineering. *Advanced materials*, 29(28):1701073, 2017.
- [13] Zhaolai Chen, Bekir Turedi, Abdullah Y Alsalloum, Chen Yang, Xiaopeng Zheng, Issam Gereige, Ahmed AlSaggaf, Omar F Mohammed, and Osman M Bakr. Single-crystal mapbi3 perovskite solar cells exceeding 21% power conversion efficiency. *ACS Energy Letters*, 4(6):1258–1259, 2019.
- [14] Jiangsheng Li, Tonggang Jiu, Chenghao Duan, Yao Wang, Hongna Zhang, Hongmei Jian, Yingjie Zhao, Ning Wang, Changshui Huang, and Yuliang Li. Improved electron transport in mapbi3 perovskite solar cells based on dual doping graphdiyne. *Nano Energy*, 46:331–337, 2018.
- [15] Yan Jiang, Emilio J Juarez-Perez, Qianqing Ge, Shenghao Wang, Matthew R Leyden, Luis K Ono, Sonia R Raga, Jinsong Hu, and Yabing Qi. Post-annealing of mapbi 3 perovskite films with methylamine for efficient perovskite solar cells. *Materials Horizons*, 3(6):548–555, 2016.
- [16] Ghada Abdelmageed, Leila Jewell, Kaitlin Hellier, Lydia Seymour, Binbin Luo, Frank Bridges, Jin Z Zhang, and Sue Carter. Mechanisms for light induced degradation in mapbi3 perovskite thin films and solar cells. *Applied Physics Letters*, 109(23):233905, 2016.
- [17] Lyubov A Frolova, Nadezhda N Dremova, and Pavel A Troshin. The chemical origin of the p-type and n-type doping effects in the hybrid methylammonium–lead iodide (mapbi 3) perovskite solar cells. *Chemical Communications*, 51(80):14917–14920, 2015.
- [18] Shuai You, Hui Wang, Shiqing Bi, Jiayu Zhou, Liang Qin, Xiaohui Qiu, Zhiqiang Zhao, Yun Xu, Yuan Zhang, Xinghua Shi, et al. A biopolymer heparin sodium interlayer anchoring tio2 and mapbi3 enhances trap passivation and device stability in perovskite solar cells. *Advanced materials*, 30(22):1706924, 2018.
- [19] Yongbo Yuan, Jungseok Chae, Yuchuan Shao, Qi Wang, Zhengguo Xiao, Andrea Centrone, and Jinsong Huang. Photovoltaic switching mechanism in lateral structure hybrid perovskite solar cells. *Advanced Energy Materials*, 5(15):1500615, 2015.
- [20] Jin Hyuck Heo, Hye Ji Han, Dasom Kim, Tae Kyu Ahn, and Sang Hyuk Im. Hysteresis-less inverted ch₃nh₃pbi₃ planar perovskite hybrid solar cells with 18.1% power conversion efficiency. *Energy & Environmental Science*, 8(5):1602–1608, 2015.
- [21] Yu Han, Steffen Meyer, Yasmina Dkhissi, Karl Weber, Jennifer M Pringle, Udo Bach, Leone Spiccia, and Yi-Bing Cheng. Degradation observations of encapsulated planar ch₃nh₃pbi₃ perovskite solar cells at high temperatures and humidity. *Journal of Materials Chemistry A*, 3(15):8139–8147, 2015.
- [22] Mingyang Cha, Peimei Da, Jun Wang, Weiyi Wang, Zhanghai Chen, Faxian Xiu, Gengfeng Zheng, and Zhong-Sheng Wang. Enhancing perovskite solar cell performance by interface engineering using ch₃nh₃pbbi₂ quantum dots. *Journal of the American Chemical*

Society, 138(27):8581–8587, 2016.

- [23] Rui Wang, Jingjing Xue, Lei Meng, Jin-Wook Lee, Zipeng Zhao, Pengyu Sun, Le Cai, Tianyi Huang, Zhengxu Wang, Zhao-Kui Wang, et al. Caffeine improves the performance and thermal stability of perovskite solar cells. *Joule*, 3(6):1464–1477, 2019.
- [24] Federico Bella, Gianmarco Griffini, Juan-Pablo Correa-Baena, Guido Saracco, Michael Grätzel, Anders Hagfeldt, Stefano Turri, and Claudio Gerbaldi. Improving efficiency and stability of perovskite solar cells with photocurable fluoropolymers. *Science*, 354(6309):203–206, 2016.
- [25] Kyoungwon Choi, Junwoo Lee, Hong Il Kim, Cheol Woong Park, Guan-Woo Kim, Hyuntae Choi, Sungjin Park, Sang Ah Park, and Taiho Park. Thermally stable, planar hybrid perovskite solar cells with high efficiency. *Energy Environ. Sci.*, 11:3238–3247, 2018.
- [26] Nam-Gyu Park. Perovskite solar cells: an emerging photovoltaic technology. *Materials today*, 18(2):65–72, 2015.
- [27] Sining Yun, Yong Qin, Alexander R Uhl, Nick Vlachopoulos, Min Yin, Dongdong Li, Xiaogang Han, and Anders Hagfeldt. New-generation integrated devices based on dye-sensitized and perovskite solar cells. *Energy & Environmental Science*, 11(3):476–526, 2018.
- [28] Jiayu Wang, Kuan Liu, Lanchao Ma, and Xiaowei Zhan. Triarylamine: versatile platform for organic, dye-sensitized, and perovskite solar cells. *Chemical reviews*, 116(23):14675–14725, 2016.
- [29] Bo Xu, Esmaeil Sheibani, Peng Liu, Jinbao Zhang, Haining Tian, Nick Vlachopoulos, Gerrit Boschloo, Lars Kloo, Anders Hagfeldt, and Licheng Sun. Carbazole-based hole-transport materials for efficient solid-state dye-sensitized solar cells and perovskite solar cells. *Advanced Materials*, 26(38):6629–6634, 2014.
- [30] Sandeep K Pathak, A Abate, P Ruckdeschel, B Roose, Karl C Gödel, Yana Vaynzof, Aditya Santhala, Shun-Ichiro Watanabe, Derek J Hollman, Nakita Noel, et al. Performance and stability enhancement of dye-sensitized and perovskite solar cells by al doping of tio2. *Advanced Functional Materials*, 24(38):6046–6055, 2014.
- [31] Bo Xu, Dongqin Bi, Yong Hua, Peng Liu, Ming Cheng, Michael Grätzel, Lars Kloo, Anders Hagfeldt, and Licheng Sun. A low-cost spirofluorene-9,9-xanthene-based hole transport material for highly efficient solid-state dye-sensitized solar cells and perovskite solar cells. *Energy Environ. Sci.*, 9:873–877, 2016.
- [32] Rui Wang, Jingjing Xue, Kai-Li Wang, Zhao-Kui Wang, Yanqi Luo, David Fenning, Guangwei Xu, Selbi Nuryyeva, Tianyi Huang, Yepin Zhao, et al. Constructive molecular configurations for surface-defect passivation of perovskite photovoltaics. *Science*, 366(6472):1509–1513, 2019.
- [33] Luciano Almeida Leal, Rafael Timóteo de Souza Júnior, Antonio Luciano de Almeida Fonseca, Luiz Antonio Ribeiro Junior, Stefan Blawid, Demetrio Antonio da Silva Filho, and Wiliam Ferreira da Cunha. Combined umc— dft prediction of electron-hole coupling in unit cells of pentacene crystals. *Journal of Molecular Modeling*, 23:153, 2017.
- [34] Vladimír Černý. Thermodynamical approach to the traveling salesman problem: An efficient simulation algorithm. *Journal of optimization theory and applications*, 45(1):41–51, 1985.
- [35] Daan Frenkel and Berend Smit. Understanding molecular simulation: From algorithms to applications, 2002.
- [36] S. Kirkpatrick, C. D. Gelatt, and M. P. Vecchi. Optimization by simulated annealing. *Science*, 220(4598):671–680, 1983.
- [37] Nicholas Metropolis, Arianna W. Rosenbluth, Marshall N. Rosenbluth, Augusta H. Teller, and Edward Teller. Equation of state calculations by fast computing machines. *The Journal of Chemical Physics*, 21(6):1087–1092, 1953.
- [38] José M Soler, Emilio Artacho, Julian D Gale, Alberto García, Javier Junquera, Pablo Ordejón, and Daniel Sánchez-Portal. The SIESTA method for ab initio order-n materials simulation. *Journal of Physics: Condensed Matter*, 14(11):2745–2779, 2002.
- [39] James P. Lewis, Kurt R. Glaesemann, Gregory A. Voth, Jürgen Fritsch, Alexander A. Demkov, José Ortega, and Otto F. Sankey. Further developments in the local-orbital density-functional-theory tight-binding method. *Phys. Rev. B*, 64:195103, Oct 2001.
- [40] N. Troullier and José Luís Martins. Efficient pseudopotentials for plane-wave calculations. ii. operators for fast iterative diagonalization. *Phys.*

Rev. B, 43:8861–8869, Apr 1991.

- [41] Warren E. Pickett. Pseudopotential methods in condensed matter applications. *Computer Physics Reports*, 9(3):115 – 197, 1989.
- [42] A. D. Becke. Density-functional exchange-energy approximation with correct asymptotic behavior. *Phys. Rev. A*, 38:3098–3100, Sep 1988.
- [43] Chengteh Lee, Weitao Yang, and Robert G. Parr. Development of the colle-salvetti correlation-energy formula into a functional of the electron density. *Phys. Rev. B*, 37:785–789, Jan 1988.
- [44] M. Barhoumi, K. Lazaar, and M. Said. Dft study of optoelectronic and magnetic properties of a novel type perovskites. *Chemical Physics*, 513:120 – 128, 2018.
- [45] Jun Yin, Partha Maity, Michele De Bastiani, Ibrahim Dursun, Osman M. Bakr, Jean-Luc Brédas, and Omar F. Mohammed. Molecular behavior of zero-dimensional perovskites. *Science Advances*, 3(12):1701793, 2017.
- [46] Hendrik J. Monkhorst and James D. Pack. Special points for brillouin-zone integrations. *Phys. Rev. B*, 13:5188–5192, Jun 1976.
- [47] WH Baur and D Kassner. The perils of cc: comparing the frequencies of falsely assigned space groups with their general population. *Acta Crystallographica Section B: Structural Science*, 48(4):356–369, 1992.
- [48] J-F Bérar and G Baldinozzi. Modeling of line-shape asymmetry in powder diffraction. *Journal of Applied Crystallography*, 26(1):128–129, 1993.
- [49] A. Boultif and D. Louër. Indexing of powder diffraction patterns for low-symmetry lattices by the successive dichotomy method. *Journal of Applied Crystallography*, 24(6):987–993, Dec 1991.
- [50] Towfiq Ahmed, C. La-O-Vorakiat, T. Salim, Yeng-Ming Lam, Elbert Chia, and Jian-Xin Zhu. Optical properties of organometallic perovskite: An ab initio study using relativistic gw correction and bethe-salpeter equation. *EPL (Europhysics Letters)*, 108, 09 2014.
- [51] Xiaohan Ke, Jun Yan, Ao Zhang, Bing Zhang, and Yunlin Chen. Optical band gap transition from direct to indirect induced by organic content of ch₃nh₃pbi₃ perovskite films. *Applied Physics Letters*, 107(9):091904, 2015.
- [52] Wei Geng, Chuan-Jia Tong, Yanning Zhang, and Li-Min Liu. Theoretical progress on the relationship between the structures and properties of perovskite solar cells. *Advanced Theory and Simulations*, 3(9):2000022, 2020.